Structure and Ferromagnetism in Carbon Nanofibers from PAN/PVP

Suminya - Teeta
Mahasarakham University https://orcid.org/0000-0003-2040-7273
Somchai - Sonsupap
Suranaree University of Technology
Ratchaneekorn - Wanchanthuek
Mahasarakham University
Santi - Maensiri
Suranaree University of Technology
Narong - Chanlek
Synchrotron Light Research Institute
Kwanruthai - Wongsaprom (wkwanruthai@gmail.com)
Mahasarakham University

Research Article

Keywords: Electrospinning, Ferromagnetic carbon , Magnetic, Nanofiber, Polymer

Posted Date: May 13th, 2021

DOI: https://doi.org/10.21203/rs.3.rs-482585/v1

Abstract

We report on the room-temperature ferromagnetism in carbon nanofibers. Carbon nanofibers were fabricated using sequential electrospinning of polyacrylonitrile (PAN) and polyvinylpyrrolidone (PVP). The morphologies, crystal structures, chemical bonding states and magnetic properties were characterized for three different polyacrylonitrile (PAN) to polyvinylpyrrolidone (PVP) weight ratios (10:0, 7:3 and 6:4) of PAN/PVP. The as-spun PAN/PVP were carbonized in three steps; stabilization, carbonization and activation at 800 ºC to obtain carbon nanofibers. The morphology and structure of the carbon nanofibers (CNFs) were completely characterized by field emission scanning electron microscopy (FE-SEM), x-ray diffraction (XRD) and Raman spectroscopy. The elemental composition and the chemical bonding of CNFs were analyzed by x-ray photoelectron spectroscopy (XPS), the magnetic properties of CNFs were measured by vibrating sample magnetometer (VSM) at room-temperature. XRD patterns showed the phase of amorphous carbon structure. The average diameter sizes of the carbon nanofibers ranged from 340 to 484 nm. Raman analysis was used to determine the carbon qualities in the samples by the numbers of sp^3/sp^2 hybridized atoms. Chemical analysis with XPS indicated that there were no magnetic contaminants in the samples. The PAN/PVP weight ratio of 6:4 showed ferromagnetic carbon nanofibers with the highest specific magnetization as ~144.2 memu/g at 300 K. These results inspire us to further research the potential of carbon materials, as a completely new class of magnetic devices. This will aid the development of new technologies in the near future.

1. Introduction

The origin of magnetism in conventional ferromagnetic materials that are composed metal elements is due to the presence of cations with partially filled *d* or *f* shells, such as iron, nickel and cobalt [1]. Ferromagnetic material can be used in many applications; including memory devices such as magnetic tapes, magnetic hard drives, and magnetic random access memory, information (magnetic recording), magnetic shielding and magnetic recording permanent magnets electromagnets core of the transformer magnetic tapes and memory store [2]. Carbon-based materials are included in the list of ferromagnetic elements that contains only *s* and *p* electrons in contrast to traditional ferromagnets [3]. Magnetism of carbon-based material has been attracting great interest due to high temperature ferromagnetic behavior and application. For application, if it is technologically feasible to produce a bulk carbon magnetic material in gram amounts, it would be expected that they would be applicable to a wide field of modern technology for medical devices; adaptable, lightweight, flexible information storage systems; have low production cost, molding capability, environmental friendliness and biocompatibility. Biotechnology applications may include biosensors, targeted drug delivery, artificial muscles, magnetic buckles, magnetic markers and magnetic resonance imaging [4–7].

Conventional, carbon-based structure were initially believed to be diamagnetic or, in special cases, paramagnetic [8]. Ferromagnetism in carbon exhibiting spontaneous magnetization at room-temperature was formerly reported as early as 1987 [9]. There have been a number of publications appearing in which erature magnetic ordering in different carbon allotropes, such

as graphite [5, 10–12], graphene [13], proton-irradiated highly oriented pyrolytic graphite (HOPG) [5, 14, 15], carbon nanotubes [6, 16, 17], polymerized fullerenes [18], carbon nanofoam [19] and amorphous carbon [20] were reported. In addition, Ma et al. [21] suggested the observation of room temperature ferromagnetism in a polymer which includes Teflon tape subjected to simple mechanical stretching, heating or cutting. Several reports have been published describing magnetism observed in carbon systems. The magnetic moments produced in carbon materials are suspected to be due to the existence of defects [5, 22]. For example, hydrogen passivated zigzag and armchair edges [23]; carbon dangling bonds or vacancy-interstitial complexes [3] [21], adatom defects [24, 25] and hydrogen adsorption defects [26] were predicted to induce local magnetic moments and magnetic order in graphite or graphene [15]. The ferromagnetism in graphitic materials has been attributed to lattice imperfections. The induction of ferromagnetism was demonstrated in proton-irradiated graphite spots [14]. The pyrolytic graphite contained a high defect concentration showing increased magnetic signals [27]. Makarova and Palacio reported that a major essential for magnetism in an all-carbon structure is the presence and stability of carbon radicals [26]. The phenomenon of radicals can introduce an unpaired spin and can bring down the potent susceptibility of pairing of all valence electrons in covalent bonds. However, the mechanism of ferromagnetism in pure carbon remains unclear [23]. Since Ovchinnikov and Spector [28] prepared ferromagnetic carbon material from polyacrylonitrile, many scientists have attempted the difficult task of reproducing ferromagnetic carbon materials. However, mostly PAN only prepared, no works have yet been reported about ferromagnetic carbon material from PAN/PVP blends, furthermore, PVP polymer is cost effective. In considering the future potential of such materials it is also necessary to take into account the lower costs of material.

In this work, the metal-free carbon materials were prepared from the mass ratios of polyacrylonitrile (PAN) and polyvinyl pyrrolidone (PVP) by electrospinning method. The all as-spuns were calcined in three steps; stabilization, carbonization and activation using a quartz tube furnace. The structural and magnetic properties of the CNFs were investigated. The CNFs are pure phase and reveal ferromagnetic behavior at room temperature. Typical characterization techniques including X-ray diffraction (XRD), Raman spectroscopy (RS), Fourier transform infrared spectroscopy (FT-IR), field emission scanning electron microscopy (FE-SEM), and vibrating sample magnetometer (VSM) were employed. Furthermore and importantly, X-ray photoelectron Spectroscopy (XPS) was performed and contributed an important role in confirming and understanding in terms of bonding configuration of the carbon system and the contamination causing a ferromagnetic behavior in the CNFs.

2. Experimental Procedure

In this study, polyacrylonitrile (M_w =150000, Aldrich) and polyvinyl pyrrolidone (M_w=1300000, Aldrich) N,N-dimethylformamide (DMF, 99.8%) were used as the starting chemicals. We first prepared three different mass ratios of PAN and PVP at 10:0, 7:3, and 6:4 in 40 ml of DMF under vigorous stirring for 5 h and with ultrasonic-assisted vibration (500W) for 30 min until a homogeneous solution was obtained. The mixed total mass of PAN and PVP in DMF was fixed to 10 wt% [29]. The PAN or PAN/PVP

electrospun fiber mats were prepared using a drum electrospinning process which is shown in Fig. 1. The voltage used for electrospinning was maintained between 15.6–16.0 kV. The distance between the syringe needle tip and the aluminum foil collector was set at 15 cm. The solution was fed at a flow rate of 0.5 ml/h. The collection of electrospun fibers was set to 6 h. All as-spun fibers were stored at room temperature. The carbon nanofibers obtained after pyrolysis of polymer fibers were placed inside a tube furnace an processes in three steps, stabilized at 280°C for 2 h in an air atmosphere at the heating rate of 2 ºC/min, and then carbonized at 500 ºC for 2 h in an argon atmosphere at the heating rate of 5 ºC/min and activation at 800°C for 2 h in an argon atmosphere at the heating rate of 5 ºC/min. Finally, the carbonized nanofibers were activated by CO_2 ambience at 800 ºC for 30 mins directly after carbonization. The carbonization samples were characterized for crystal phase identification by X-ray diffractometer (XRD) (Advance Bruker D8, Germany) with Cu-Kα radiation (λ= 0.15406 nm). The morphology and average diameter of carbonization samples were characterized by field emission scanning electron microscopy (FE-SEM; Helios Nanolab G3 CX). The chemical bonding and elemental composition of CNFs were analyzed by X-ray photoelectron spectroscopy (XPS) (ULVAC-PHI, Japan) with Al K (1486.4 eV) radiation as the excitation source. The functional groups were characterized by Fourier transform infrared spectroscopy (FT-IR) (Bruker Tensor 27, U.K). Characterization of the crystalline perfection of graphite-based samples employed Raman spectroscopy (Bruker, MultiRAM and SENTERRA II, UK). The magnetic measurements were investigated at room temperature using a vibration sample magnetometer (Versalab^{TM} Tesla VSM 7403, USA).

3. Results And Discussion

The morphology of nanofibers was analyzed by FE-SEM. Figure 2a, b and c show the morphology of the as-spun pure PAN nanofibers, PAN/PVP (7:3) and PAN/PVP (6:4) obtained after electrospinning. The average diameter of nanofibers could be measured and calculated by the software ImageJ and Microsoft Excel. The average diameter of fibers changed with the different PAN/PVP ratios. All samples exhibited a smooth surface and were continuous cylindrical and the average diameter of nanofibers was around 474 ± 76 to 740 ± 75 nm. Figure 2d, e and f show the morphology of the pure PAN nanofibers, PAN/PVP (7:3) and PAN/PVP (6: 4) obtained after carbonization at 800°C; their diameters were 511 ± 81, 440 ± 63, and 340 ± 60 nm, respectively. This average diameter was measured just on the fibrous morphology, it was not in interconnection areas. The reduction in average diameter of the nanofibres after calcination could be attributed to the loss of PVP and PAN from the nanofibers [29–31]. The average diameter of samples has been found to decrease with increasing the PVP content because PVP completely degrades during the carbonization process. However, the size of fibers could be increased with the PVP content because of fiber-fiber interconnection. Niu et al.[30] reported that fiber diameter increased with the PAN/PVP ratio at 13:87 and 8:92. There was almost no fiber – fiber interconnection at a low PVP content. In this case the interconnection fiber was formed only in small areas, which were mostly invisible, explaining why the fiber diameter decreased with the PVP content.

Figure 3 shows the XRD pattern of all samples used for investigation of their crystal structures. For all samples, diffraction peaks corresponding to the (002) and (101) peaks of graphitic carbon were observed at approximately 2θ = 25° and 44° [20]. The broad diffraction peaks suggest the disorder and amorphous characteristics of the materials [32]. These results imply that the crystal structure of PAN and PAN/PVP nanofibers is not changed by increasing PVP content; only the intensity is changed, which in the sample PAN/PVP (6:4) is the lowest intensity and is in agreement with the previous report by Lv et al. [33]. This may result from the incorporation of carbon nanoparticles from PVP into the sample. The decrease in terms of diffraction peaks led to a decrease of degree of crystallinity of PAN/PVP nanofiber [34], but it is far from the perfect graphitized structure [35].

The surface elemental composition and their binding energies of samples were investigated by X-ray photoelectron spectroscopy (XPS). The main peak contained two distinct peaks, indicating the existence of carbon and oxygen elements as shown in Fig. 4. From the survey spectra, the intensity of O1s peak of PAN/PVP(6:4) sample was much stronger compared with the O1s of PAN. This result obviously indicated increased oxygen functional groups in of PAN/PVP(6:4). Figure 5a-c shows that the high-resolution C1s spectrum of all samples can be deconvolved into three peaks centered attributed to C-C and/or C = C ranging 284.6-284.8 eV [36–38] that originated from the sp^3 C-C bond, C–O and/or C-OH ranging 286.0-286.7 eV, and O–C = O ranging 287.6-289.5 eV [39]. The results show the proportion of C-C/C = C, C-O-C and O-C = O decreased in the order of PAN/ PVP (6:4) > PAN > PAN/ PVP (7:3) (see Fig. 5d, e, and f). The O1s spectra of all samples deconvolved into two main peaks attributed to C = O and ranging from 531.1-531.8 eV and C–O ranging 532.4-533.2 eV (see Fig. 6a, b, and c) [7]. The comparison of the proportion of C = O and C-O in all samples is shown in Fig. 6d and e. FT-IR spectra was characterized in the samples in order to understand the relevant functional groups after the heat treatment activity. For comparison, pure PAN and PAN/PVP show the absorption peak Fig. 7. The FT-IR spectra show that the PVP had no effect on the functional groups in the samples, which were similar in the appearance; however, a small shift in PAN/PVP (6:4) towards the higher wavenumber observed and may be due to incorporation of carbon nanoparticles in the template. The broad absorption band at ~ 1160 cm^{-1} represents the stretching mode of C-O from the carboxyl group (-COOH) [40]. The peak at 1563 cm^{-1} represents the stretching mode of the C = C group from an aromatic ring [41, 42]. The band at ~ 1800 cm^{-1} may be assigned to the C = O bond stretching vibration mode [43–45]. The peak at 1892 cm^{-1} is assigned to the aromatic combination band [46]. The peak around 2082 cm^{-1} indicates the C ≡ C bending [47].

Raman analysis was used to determine the carbon quality of PAN and PAN/PVP (6:4) samples by using a Gaussian fitting of the observed band positions. In addition, Raman spectroscopy is a commonly used technique for identifying secondary phase in doped/composites materials. The first-order zone boundary phonon mode component with D and G band, D band has sp^3 carbon bonded (C-C), associated with the disorder that was induced by defects (vacancies) in the carbon nanofibers. The G band results from the stretching of the C = C bonds in the hexagonal ring of sp^2 bonded carbon in graphitic structures [32, 48]. Figure 8a and b show the D bands associated with PAN and PAN/PVP (6:4) are located at 1361.2 and [illegible] d peaks at 1580.5 and 1581.8 cm^{-1} that corresponded to an

ideal graphitic lattice vibration mode with E_{2g} symmetry [49]. The intensity ratio of D band to G band (R = I_D/I_G) reflects the degree of the defects in the carbon nanofibers. This work showed an I_D/I_G ratio of 1.78 for PAN obtained from the fitting (see Fig. 8a). The I_D/I_G value of carbon nanofibers increased to 1.89 with decreasing ratio of PAN/PVP(6:4) (see Fig. 8b). The comparison of spectra for PAN and PAN/PVP96:4) is shown in Fig. 8c. An increase in the I_D/I_G ratio indicates an increase in the number of defects on nanofibers, which indicates the decrease in the average diameter size from the FE-SEM result [43]. The observed Raman bands around 2704 and 2870 cm^{-1} are assigned to the secondary order zone boundary phonon mode component that related to the phonon oscillation in the infinite crystal of graphite structure for the samples of PAN and PAN/PVP(6:4) respectively [50]. No additional peaks of impurities are observed in the spectrum. From, the information of surface functional groups obtained by XPS, FT-IR and Raman, the result suggested agreement in C = O, C-O and C ≡ C. The result indicated that the surface of carbon nanofibers contained C-C/C = C, C-O, and C = O.

The specific magnetization (M–H curves) of PAN and PAN/PVP carbon nanofibers were obtained at room temperature. The VSM measurement in Fig. 9 (a to d) shows that the magnetic hysteresis loops with applied magnetic field cycled between − 15000 and 15000 Oe. The samples exhibited magnetic behavior after subtracting the diamagnetic contribution from the gel cap sample holder. The M-H curve of all samples are representative for a magnetic material and indicate hysteresis in ferromagnetic component in the field ranges of ± 5000 Oe, while outside this range, the specific magnetization slightly increases with increasing field. The specific magnetization values of 34.7, 7.7, and 144.2 memu/g and coercivity of 949.6, 1763.5 and 2777.0 Oe were observed for the PAN, PAN/PVP (7:3) and PAN/PVP (6:4) samples, respectively (Table 1). The coercivity is the demagnetizing field needed to reduce the remnant magnetization to zero [51]. This study shows that the coercivity values of samples increased with average fiber diameter and the increase of oxygen function groups attached on the surface. The ferromagnetic component increases in an unusual manner related to increasing the content of PVP in samples, when the increasing of PAN/PVP (7:3) leading to decrease in a specific magnetization of magnitude. According to our XPS results, the C:O ratios of the PAN, PAN/PVP(7:3) and PAN/PVP(6:4) were 87.95:12.05, 92.98:7.02 and 89.78:10.22, respectively. The proportion of C = O and C-O decreased in the order of PAN/ PVP (6:4) > PAN > PAN/ PVP (7:3) (see Fig. 6d and e). The oxygen coverage was small in PAN/ PVP(7:3) so that it was possible for magnetic ordering to occur because the magnetic domain could develop in graphite oxide [52], while increasing of PAN/PVP (6:4) leading to an increase in a specific magnetization of content that shows the highest magnetic moment of our sample. This may be due to increasing amorphization that correlated with the increasing ratio of I_D/I_G from Raman analysis. The I_D/I_G is monotonically increased with the PVP content, which indicates an increased density of vacancy defects [5]. The results show that the amount of vacancy in samples tends to increase with PVP content. The vacancy in samples is predicted to have local magnetic moments [53], the local moments could couple each other and produce a long-range order, and could give rise to ferromagnetic behavior in samples, which explained the increase in the magnetization in the PAN/PVP(6:4) sample. Furthermore, the carbon atoms neighboring to defects in samples will adjust their bonds to accommodate the defects

 erates a magnetic moment. Thus, the origin of the

ferromagnetism was suggested to be attributed to the mixture of carbon atoms with sp^2 and sp^3 bonds according to the above XPS and Raman analysis, and this creates vacancies in the presence of unpaired electron spins in sp^3 carbon bonds that contributed the ferromagnetism [10, 54], In addition, the FE-SEM shows the smallest average diameter of nanofibers were possible magnetically ordered due to the large amount of graphitized carbons edge sites magnetism [20, 55]. The observed ferromagnetism could be based on the rich carbon defects of carbon dangling bonds and strong ferromagnetic coupling between them [3]. This suggest that the increasing disorder in the graphite structure in samples clearly played an important role in improving the ferromagnetic properties of graphite, in agreement with the results of the ratio of I_D/I_G [51]. This observation is consistent with previous research results of Saito et al [11] reported that the carbon material prepared by pyrolysis of PAN at 1273 K for 1 h that was attracted by the permanent magnet and which is a ferromagnetic carbon material. The authors suggested that the ferromagnetic behavior in carbon exhibited a saturation magnetization of 1.22 emu/g at 300 K.

Table 1
The magnetization and coercivity of carbon nanofiber from PAN and PAN/ PVP blend for different concentration.

Samples	Average diameter (nm)	M (memu/g)	H_c (Oe)
PAN	511 ± 81	34.7	949.6
PAN/PVP (7:3)	440 ± 63	7.7	1763.5
PAN/PVP (6:4)	340 ± 60	144.2	2777.0

4. Conclusion

In this study, we report the existence of room temperature ferromagnetism in carbon nanofibers. The carbon nanofibers were prepared by an electrospinning technique and carbonization of PAN and PVP at high temp, which is an easy and low-cost process. The as-spuns were carbonized at 800 ºC to obtain a carbon nanofibers by three steps of stabilization, carbonization and activation. The PAN/PVP weight ratio of 6:4 was shown to have ferromagnetic carbon nanofibers with the highest specific magnetization of ~ 144.2 memu/g at 300 K. Chemical analysis with XPS indicated that there was no magnetic impurity in the samples. The ferromagnetic behavior reported here is considered to be associated with the mixed fraction of sp^2 and sp^3 carbon atom in carbon nanofibers; furthermore the nanostructure could also play an important role in the net magnetic moment obtained. These results inspire us to further research the potential of carbon materials as a completely new class and generation of magnetic devices with, for instance, low mass density or biocompatibiliy. This will aid the development of new technologies in the near future.

Declarations

Acknowledgments

The authors would like to thank the Synchrotron Light Research Institute (BL5) (Public Organization), Nakhon Ratchasima, Thailand, for XPS facilities. The Department of Physics, Faculty of Science, Khon Kean University for providing VSM facilities. This work was supported by Thailand Research Fund (Contact No. MRG6080262).

References

1. J. M. D. Coey, d^0 Ferromagnetism, Solid State Sci. **7**(6), 660–667 (2005). https://doi: 10.1016/j.solidstatesciences.2004.11.012
2. A. Goldman and A. Goldman, Applications and Functions of Ferromagnetic Materials, Handb. Mod. Ferromagn. Mater. 1–15 (1999).https://doi: 10.1007/978-1-4615-4917-8_1
3. X. L. Wu et al., Room temperature ferromagnetism in naphthalene, Carbon N. Y. **136**, 125–129 (2018). https://doi: 10.1016/j.carbon.2018.04.078
4. T. L. Makarova, Ferromagnetic Carbonaceous Compounds, Carbon Based Magn. 541–562 (2006). https://doi: 10.1016/B978-044451947-4/50025-6
5. Z. He, H. Xia, X. Zhou, X. Yang, Y. Song, and T. Wang, Raman study of correlation between defects and ferromagnetism in graphite, J. Phys. D. Appl. Phys. **44**(8), (2011). https://doi: 10.1088/0022-3727/44/8/085001
6. S. Okada, K. Nakada, K. Kuwabara, K. Daigoku, and T. Kawai, Ferromagnetic spin ordering on carbon nanotubes with topological line defects, Phys. Rev. B - Condens. Matter Mater. Phys.**74**(12), 2–5 (2006). https://doi: 10.1103/PhysRevB.74.121412
7. D. Xiang, X. Liu, and X. Dong, A facile synthetic method and electrochemical performances of nickel oxide/carbon fibers composites, J. Mater. Sci. **52**(13), 7709–7718 (2017). https://doi: 10.1007/s10853-017-1019-4
8. P. Esquinazi and R. Höhne, Magnetism in carbon structures, J. Magn. Magn. Mater. 290-291, 20–27 (2005). https://doi: 10.1016/j.jmmm.2004.11.154
9. R. Caudillo, X. Gao, R. Escudero, M. José-Yacaman, and J. B. Goodenough, Ferromagnetic behavior of carbon nanospheres encapsulating silver nanoparticles, Phys. Rev. B - Condens. Matter Mater. Phys. **74**(21), 1–12 (2006). https:// doi: 10.1103/PhysRevB.74.214418
10. J. Červenka, M. I. Katsnelson, and C. F. J. Flipse, Room-temperature ferromagnetism in graphite driven by two-dimensional networks of pointdefects, Nat. Phys. **5**(11), 840–844 (2009).https://doi: 10.1038/nphys1399
11. T. Saito, D. Nishio-Hamane, S. Yoshii, and T. Nojima, Ferromagnetic carbon materials prepared from polyacrylonitrile, Appl. Phys. Lett. **98**(5), 12–15 (2011). https://doi: 10.1063/1.3551522
12. H. Pardo et al., Raman characterization of bulk ferromagnetic nanostructured graphite, Phys. B Condens. Matter. **407**(16), 3206–3209 (2012).https://doi: 10.1016/j.physb.2011.12.066

13. S. S. Rao et al., Ferromagnetism in graphene nanoribbons: Split versus oxidative unzipped ribbons, Nano Lett. **12**(3), 1210–1217 (2012).https://doi: 10.1021/nl203512c
14. P. Esquinazi, D. Spemann, R. Höhne, A. Setzer, K. H. Han, and T. Butz, Induced magnetic ordering by proton irradiation in graphite, Phys. Rev. Lett. **91**(22), 8–11 (2003). https://doi: 10.1103/PhysRevLett.91.227201
15. X. Yang et al., Correlation between the vacancy defects and ferromagnetism in graphite, Carbon N. Y. **47**(5), 1399–1406 (2009).https://doi: 10.1016/j.carbon.2009.01.032
16. Z. Zanolli and J. C. Charlier, Spin transport in carbon nanotubes with magnetic vacancy-defects, Phys. Rev. B - Condens. Matter Mater. Phys. **81** (16), (2010). https://doi: 10.1103/PhysRevB.81.165406
17. U. Weissker, S. Hampel, A. Leonhardt, and B. Büchner, Carbon nanotubes filled with ferromagnetic materials, Materials (Basel). **3**(8), 4387–4427 (2010). https://doi: 10.3390/ma3084387
18. H. Ohldag et al., Π-Electron Ferromagnetism in Metal-Free Carbon Probed By Soft X-Ray Dichroism, Phys. Rev. Lett. **98**(18), (2007).https://doi: 10.1103/PhysRevLett.98.187204
19. S. Talapatra et al., Irradiation-induced magnetism in carbon nanostructures, Phys. Rev. Lett. **95** (9), (2005). https://doi: 10.1103/PhysRevLett.95.097201.
20. A. Komlev, E. Lähderanta, E. Shevchenko, and N. Vorob'ev-Desyatovskii, Magnetism of purified amorphous carbon, EPJ Web Conf, **185,** 8–11 (2018). https://doi: 10.1051/epjconf/201818504012
21. Y. W. Ma et al., Room temperature ferromagnetism in Teflon due to carbon dangling bonds, Nat. Commun. **3**, (2012). https://doi: 10.1038/ncomms1689
22. E. Lähderanta, A. V. Lashkul, K. G. Lisunov, D. A. Zherebtsov, D. M. Galimov, and A. N. Titkov, Magnetic properties of carbon nanoparticles, IOP Conf. Ser. Mater. Sci. Eng. **38**(1), (2012).https://doi: 10.1088/1757-899X/38/1/012010
23. G. Z. Magda et al., Room-temperature magnetic order on zigzag edges of narrow graphene nanoribbons, Nature. **514**(7524), 608–611 (2014). https://doi: 10.1038/nature13831
24. P. O. Lehtinen, A. S. Foster, A. Ayuela, A. Krasheninnikov, K. Nordlund, and R. M. Nieminen, Magnetic Properties and Diffusion of Adatoms on a Graphene Sheet, Phys. Rev. Lett. **91**(1), 1–4 (2003).https://doi: 10.1103/PhysRevLett.91.017202
25. Y. Zhang, S. Talapatra, S. Kar, R. Vajtai, S. K. Nayak, and P. M. Ajayan, First-principles study of defect-induced magnetism in carbon, Phys. Rev. Lett. **99**(10), 1–4 (2007). https://doi: 10.1103/PhysRevLett.99.107201
26. O. V. Yazyev and L. Helm, Defect-induced magnetism in graphene, Phys. Rev. B - Condens. Matter Mater. Phys. **75**(12), 1–5 (2007).https://doi: 10.1103/PhysRevB.75.125408
27. P. Esquinazi et al., Ferromagnetism in oriented graphite samples, Phys. Rev. B - Condens. Matter Mater. Phys. **66**(2), 1–10 (2002).https://doi: 10.1103/PhysRevB.66.024429
28. A. A. Ovchinnikov and V. N. Spector, Organic ferromagnets. New results, Synth. Met. **27**(3–4), 615–624 (1988). https://doi: 10.1016/0379-6779(88)90208-1

29. G. H. An, B. R. Koo, and H. J. Ahn, Activated mesoporous carbon nanofibers fabricated using water etching-assisted templating for high-performance electrochemical capacitors, Phys. Chem. Chem. Phys. **18**(9), 6587–6594 (2016). https://doi: 10.1039/c6cp00035e
30. H. Niu, J. Zhang, Z. Xie, X. Wang, and T. Lin, Preparation, structure and supercapacitance of bonded carbon nanofiber electrode materials, Carbon N. Y. **49**(7), 2380–2388 (2011). https://doi: 10.1016/j.carbon.2011.02.005
31. O. Pech and S. Maensiri, Electrochemical performances of electrospun carbon nanofibers, interconnected carbon nanofibers, and carbon-manganese oxide composite nanofibers, J. Alloys Compd. **781**, 541–552 (2019). https://doi: 10.1016/j.jallcom.2018.12.088
32. S. Ma et al., Magnetism of amorphous carbon nanofibers, Appl. Phys. Lett. **95**, 1–4 (2009). https://doi: 10.1063/1.3272940
33. J. Lv, W. Gu, X. Cui, S. Dai, B. Zhang, and G. Ji, Nanofiber network with adjustable nanostructure controlled by PVP content for an excellent microwave absorption, Sci. Rep. **9**(1), 2–11 (2019).https://doi: 10.1038/s41598-019-38899-8
34. O. Mukongo Mpukuta, K. Dincer, and M. Okan Erdal, Investigation of electrical conductivity of PAN nanofibers containing silica nanoparticles produced by electrospinning method, Mater. Today Proc. **18**, 1927–1935 (2019). https://doi: 10.1016/j.matpr.2019.06.683
35. G. Wang et al., Activated carbon nanofiber webs made by electrospinning for capacitive deionization, Electrochim. Acta, **69,** 65–70 (2012). https://doi: 10.1016/j.electacta.2012.02.066
36. Z. Yue, K. R. Benak, J. Wang, C. L. Mangun, and J. Economy, Elucidating the porous and chemical structures of ZnCl 2-activated polyacrylonitrile on a fiberglass substrate, J. Mater. Chem. **15**(30), 3142–3148 (2005). https://doi: 10.1039/b504141d
37. L. Pérez-Álvarez, L. Ruiz-Rubio, I. Moreno, and J. L. Vilas-Vilela, Characterization and optimization of the alkaline hydrolysis of polyacrylonitrile membranes, Polymers (Basel). **11**(11), 1–11 (2019). https://doi: 10.3390/polym11111843
38. B. Xu et al., What is the choice for supercapacitors: Graphene or graphene oxide, Energy Environ. Sci. **4**(8), 2826–2830 (2011). https://doi: 10.1039/c1ee01198g
39. E. N. Attia, F. M. Hassan, M. Li, R. Batmaz, A. Elkamel, and Z. Chen, Tailoring the chemistry of blend copolymers boosting the electrochemical performance of Si-based anodes for lithium ion batteries, J. Mater. Chem. A. **5**(46), 24159–24167 (2017). https:// doi: 10.1039/c7ta08369f
40. V. Ţucureanu, A. Matei, and A. M. Avram, FTIR Spectroscopy for Carbon Family Study, Crit. Rev. Anal. Chem. **46**(6), 502–520 (2016). https://doi: 10.1080/10408347.2016.1157013
41. A. C. Obreja et al., Isocyanate functionalized graphene/P3HT based nanocomposites, Appl. Surf. Sci. **276,** 458–467 (2013). https://doi: 10.1016/j.apsusc.2013.03.117
42. C. Liu and K. Lafdi, Fabrication and characterization of carbon nanofibers from polyacrylonitrile/pitch blends, J. Appl. Polym. Sci. **134**(42), 1–7 (2017). https://doi: 10.1002/app.45388

43. N. B. A. Mansor, J. P. Tessonnier, A. Rinaldi, S. Reiche, and M. G. Kutty, Chemically modified multi-walled carbon nanotubes (MWCNTs) with anchored acidic groups, Sains Malaysiana. **41**(5), 603–609 (2012)
44. V. A. E. Barrios, J. R. R. Méndez, N. V. P. Aguilar, G. A. Espinosa, and J. L. D. Rodríguez, FTIR - An Essential Characterization Technique for Polymeric Materials, Infrared Spectrosc. - Mater. Sci. Eng. Technol, Prof. Theophanides Theophile (Ed.). 195-210 (2012). https://doi: 10.5772/36044.
45. M. R. Johan, S. H. Meriam Suhaimy, and Y. Yusof, Physico-chemical studies of cuprous oxide (Cu_2O) nanoparticles coated on amorphous carbon nanotubes (α-CNTs), Appl. Surf. Sci. **289**, 450–454 (2014). https://doi: 10.1016/j.apsusc.2013.11.002
46. J. Coates, Interpretation of Infrared Spectra, A Practical Approach, Encycl. Anal. Chem.1–23 (2006). https://doi: 10.1002/9780470027318.a5606
47. F. E. C. Othman et al., Preparation and characterization of Polyacrylonitrile/ Manganese Dioxides-based Carbon Nanofibers via electrospinning process, IOP Conf. Ser. Earth Environ. **36**(1), (2016). https://doi: 10.1088/1755-1315/36/1/012006
48. J. Yan, Q. Wang, T. Wei, and Z. Fan, Recent advances in design and fabrication of electrochemical supercapacitors with high energy densities, Adv. Energy Mater. **4**(4), (2014). https://doi: 10.1002/aenm.201300816
49. A. Sadezky, H. Muckenhuber, H. Grothe, R. Niessner, and U. Pöschl, Raman microspectroscopy of soot and related carbonaceous materials: Spectral analysis and structural information, Carbon N. Y. **43**(8), 1731–1742 (2005). https://doi: 10.1016/j.carbon.2005.02.018
50. M. A. Pimenta, G. Dresselhaus, M. S. Dresselhaus, L. G. Cançado, A. Jorio, and R. Saito, Studying disorder in graphite-based systems by Raman spectroscopy, Phys. Chem. Chem. Phys. **9**(11), 1276–1291 (2007). https://doi: 10.1039/b613962k
51. R. N. Bhowmik, Ferromagnetism in lead graphite-pencils and magnetic composite with $CoFe_2O_4$ particles, Compos. Part B Eng. **43**(2), 503–509 (2012). https://doi: 10.1016/j.compositesb.2011.07.013
52. D. Lee and J. Seo, Magnetic frustration of graphite oxide, Sci. Rep. **7**, 2–7 (2017). https://doi: 10.1038/srep44690
53. P. O. Lehtinen, A. S. Foster, Y. Ma, A. V. Krasheninnikov, and R. M. Nieminen, Irradiation-induced magnetism in graphite: A density functional study, Phys. Rev. Lett. **93**(18), 1–4 (2004).https://doi: 10.1103/PhysRevLett.93.187202
54. A. Sinha, A. Ali, and A. D. Thakur, Ferromagnetism in graphene oxide, Mater. Today Proc. 8–11 (2020). https://doi: 10.1016/j.matpr.2020.04.771
55. T. Ishii et al., Analyses of trace amounts of edge sites in natural graphite, synthetic graphite and high-temperature treated coke for the understanding of their carbon molecular structures, Carbon N. Y. **125**, 146–155 (2017). https://doi: 10.1016/j.carbon.2017.09.049

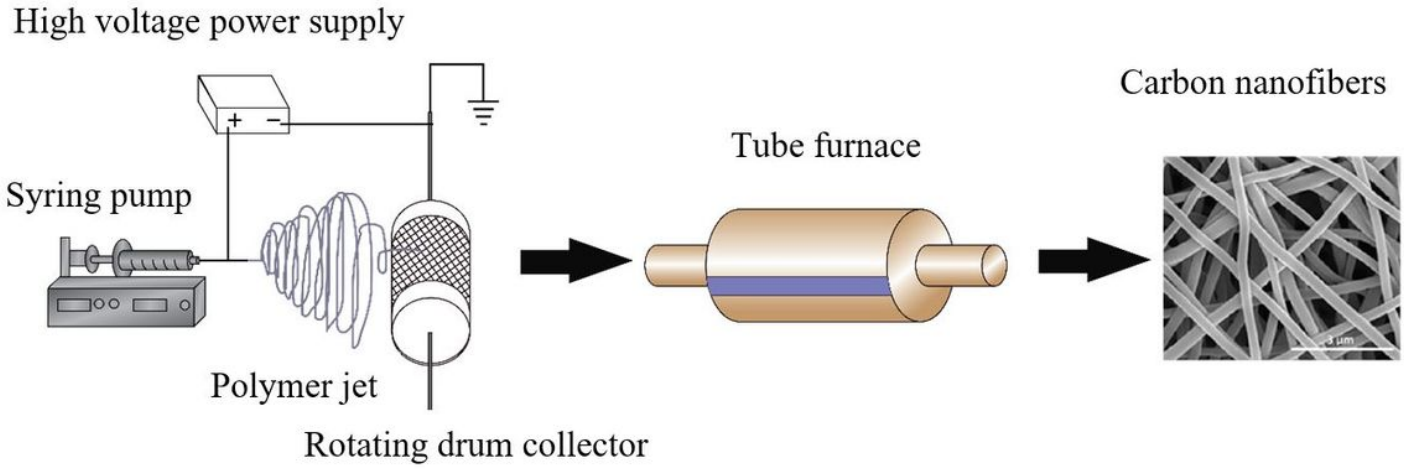

Figure 1

Schematic diagram setup for the electrospinning of carbon nanofibers.

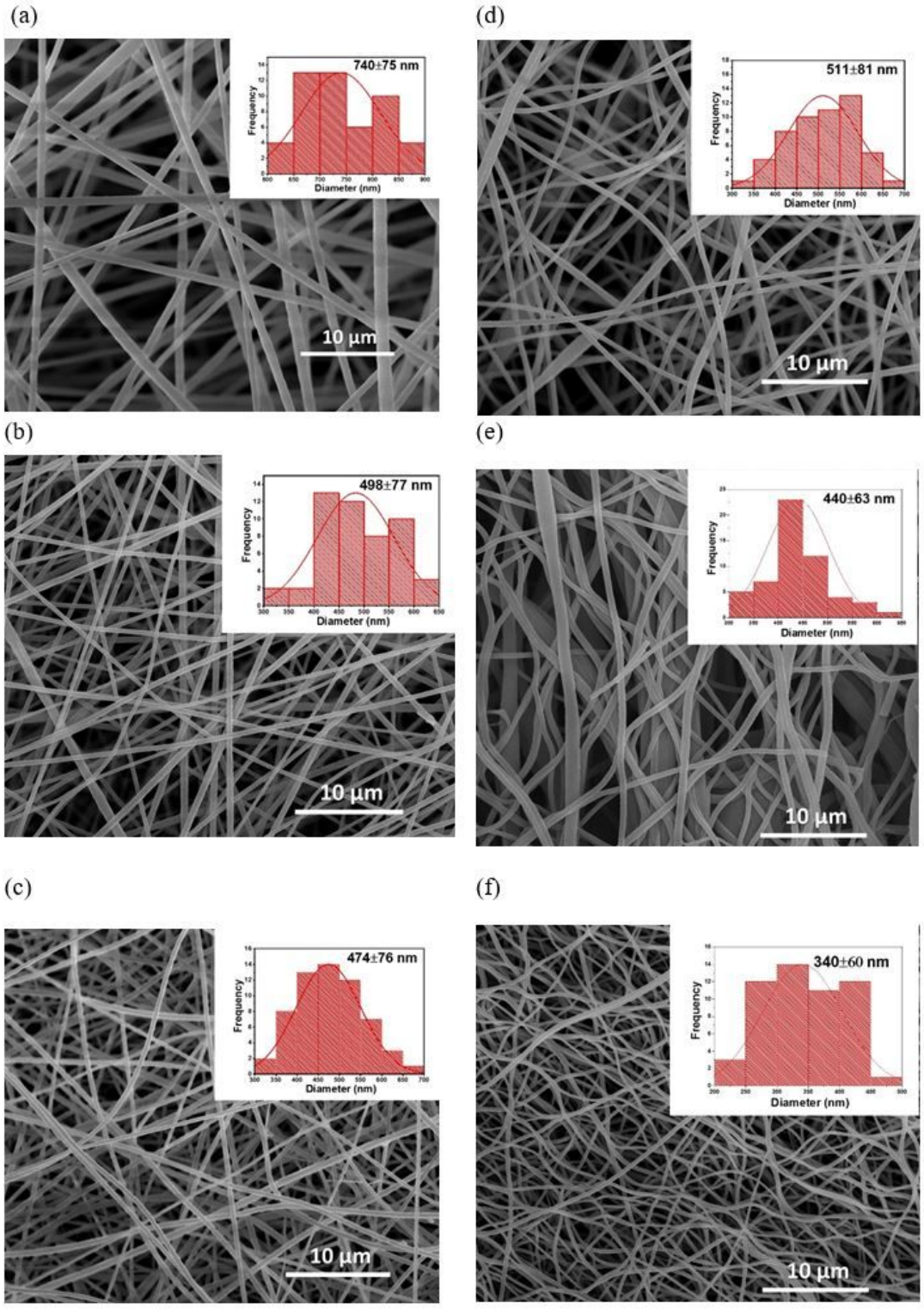

Figure 2

FE-SEM image of as-spun (a) PAN (b) PAN/ PVP (7:3) (c) PAN/ PVP (6:4) and after carbonized at 800°C for 2 h (d) PAN (e) PAN/ PVP (7:3) and (f) PAN/ PVP (6:4).

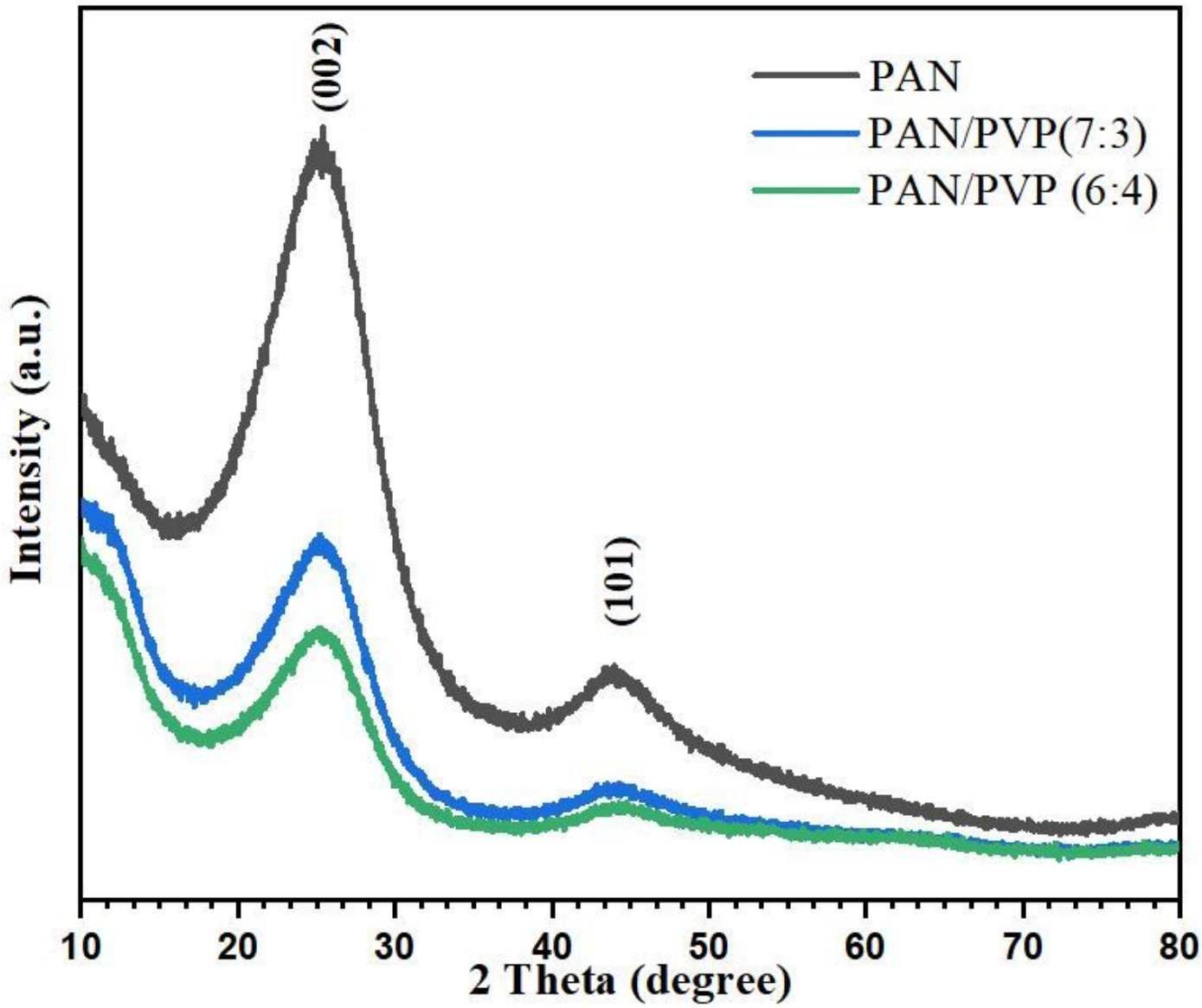

Figure 3

XRD patterns of carbon nanofiber from PAN and PAN mixed PVP in different ratio after carbonized at 800°C for 2 h.

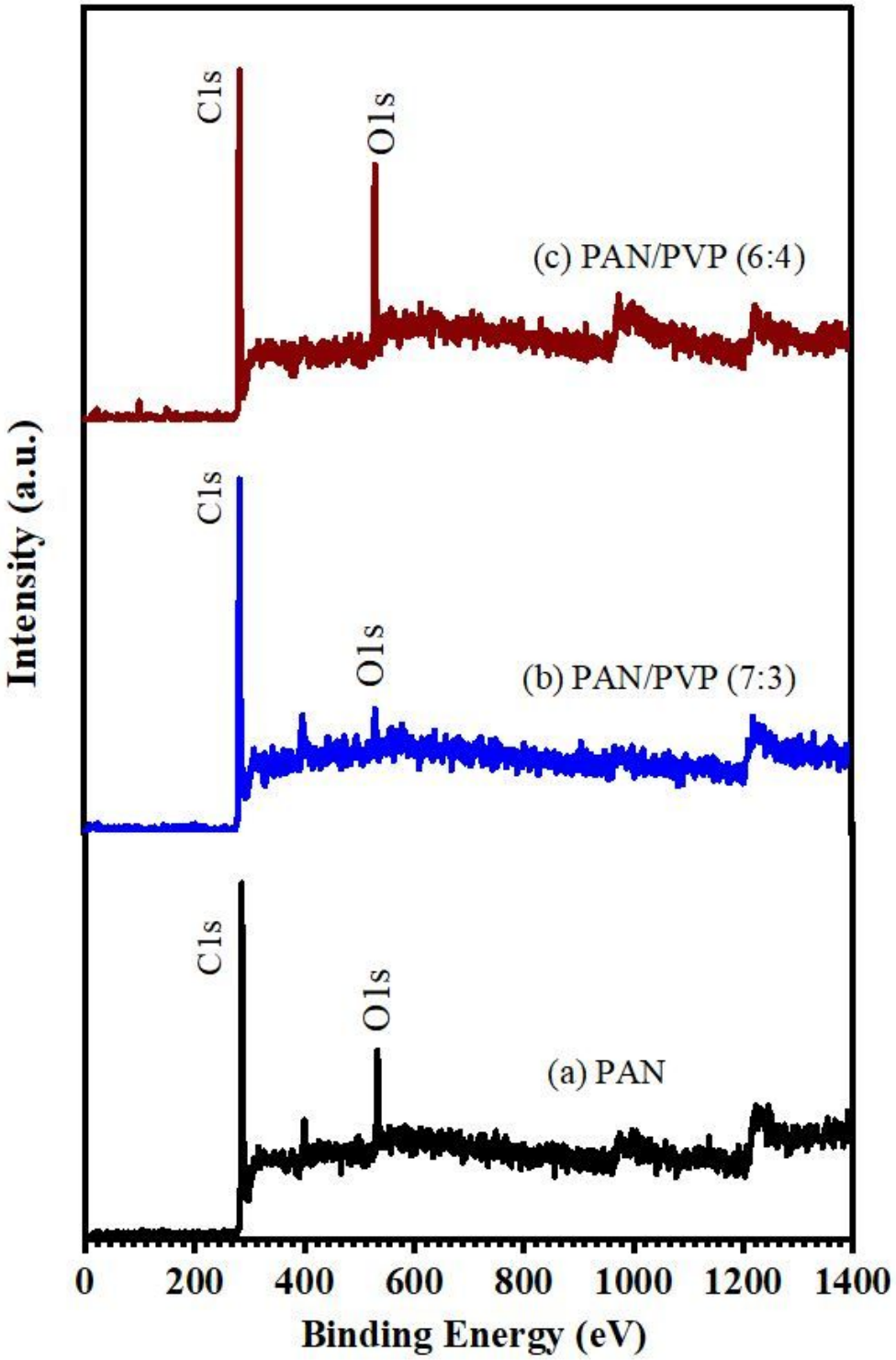

Figure 4

XPS survey spectra of carbon nanofiber from PAN and PAN mixed PVP (a) PAN (b) PAN/ PVP (7:3) and (c) PAN/ PVP (6:4) in different ratio carbonized nanofibers at 800°C for 2 h.

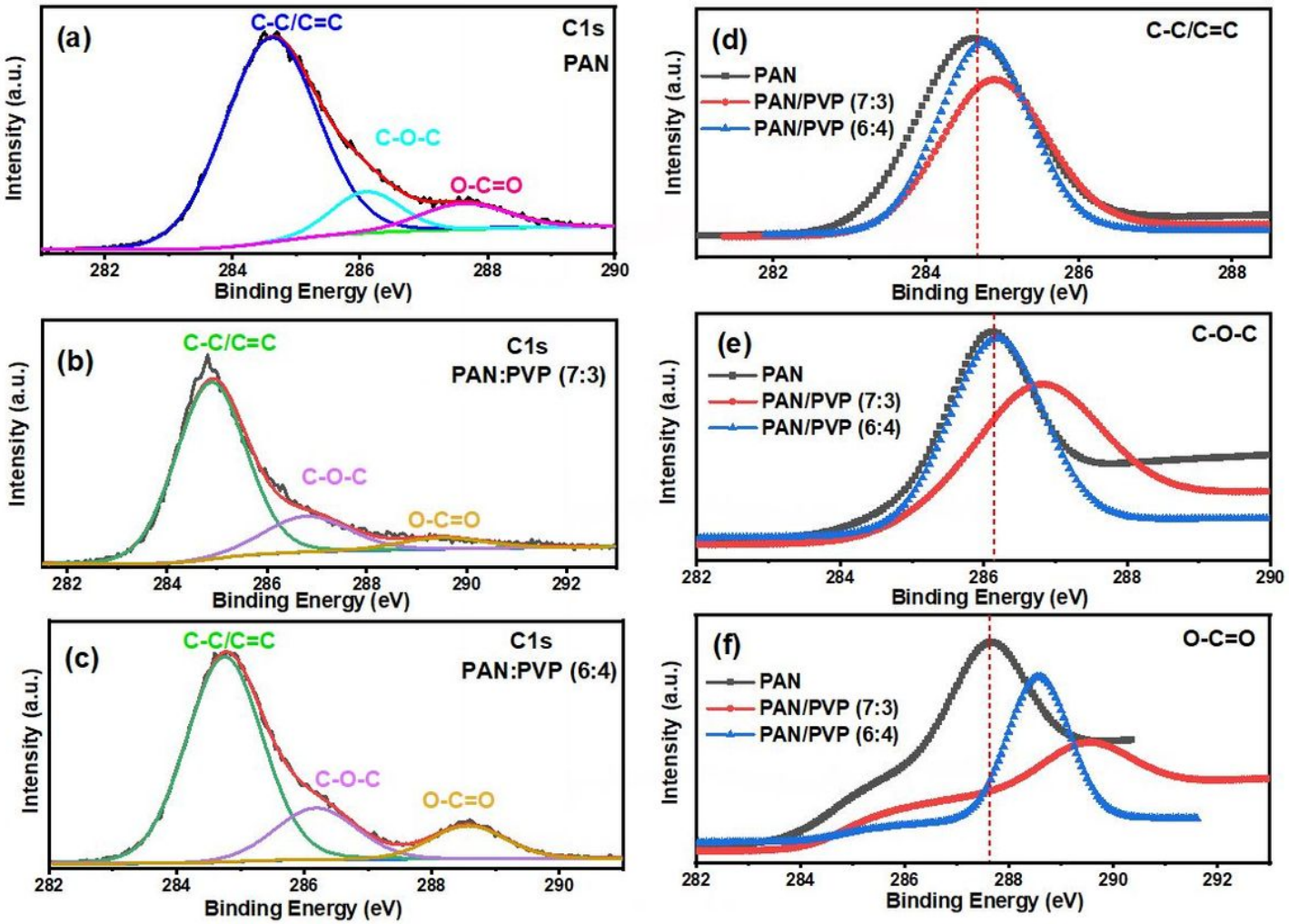

Figure 5

XPS C1s spectra and fitting curves of carbon nanofiber from PAN and PAN mixed PVP (a) PAN (b) PAN/ PVP (7:3) (c) PAN/ PVP (6:4) in different ratio carbonized nanofibers at 800°C for 2 h. The proportion for comparison of (d) C-C/C=C (e) C-O-C and (f) O-C=O in PAN, PAN/ PVP (7:3) and PAN/ PVP (6:4).

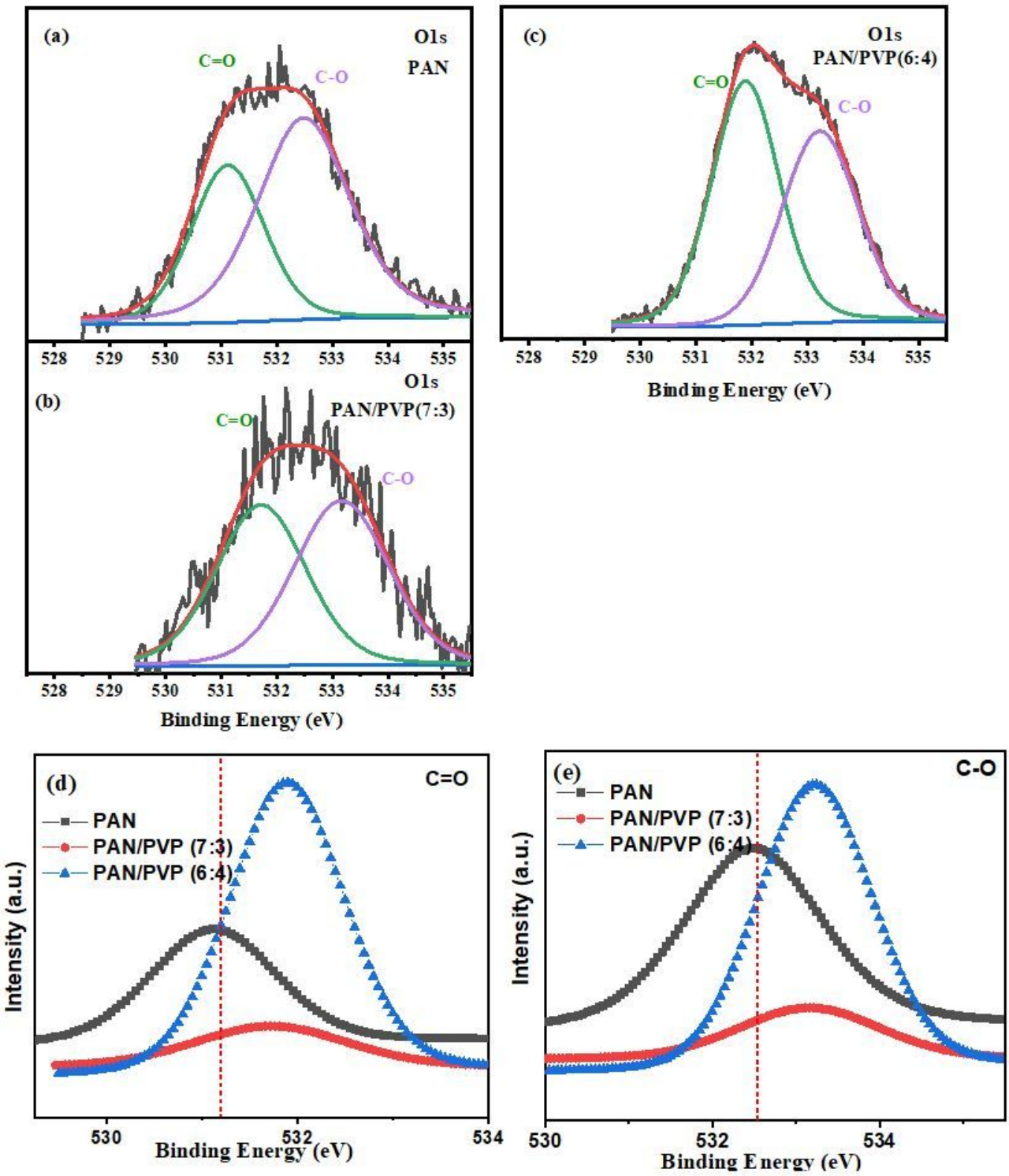

Figure 6

XPS O1s spectra and fitting curves of carbon nanofiber from PAN and PAN mixed PVP (a) PAN (b) PAN/ PVP (7:3) and (c) PAN/ PVP (6:4) in different ratio carbonized nanofibers at 800°C for 2 h. The proportion for comparison of (d) C=O and (e) C-O in PAN, PAN/ PVP (7:3) and PAN/ PVP (6:4).

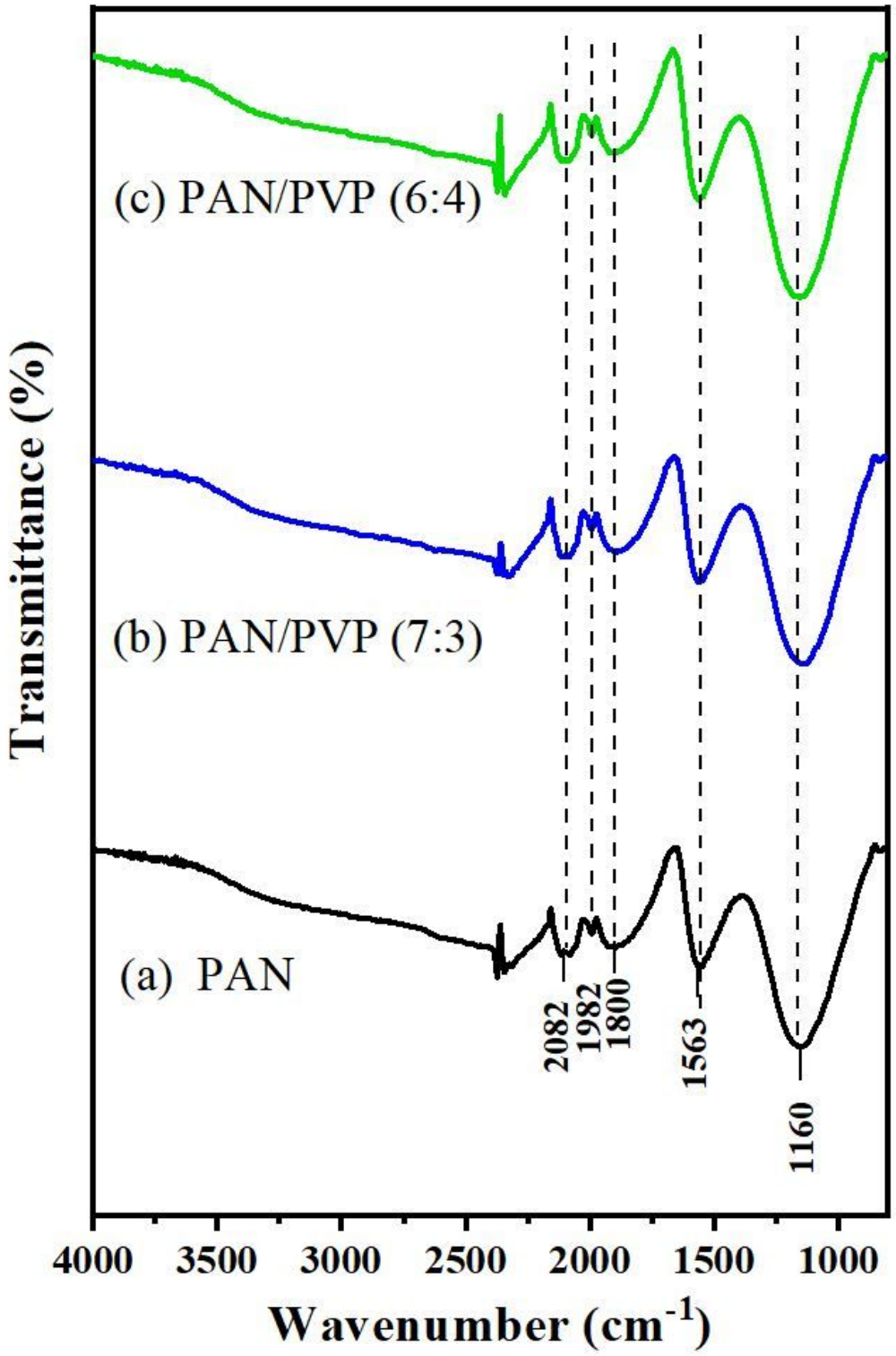

Figure 7

FT-IR spectra of carbon nanofiber from PAN and PAN mixed PVP (a) PAN (b) PAN/ PVP (7:3) and (c) PAN/ PVP (6:4) in different ratio carbonized nanofibers at 800°C for 2 h.

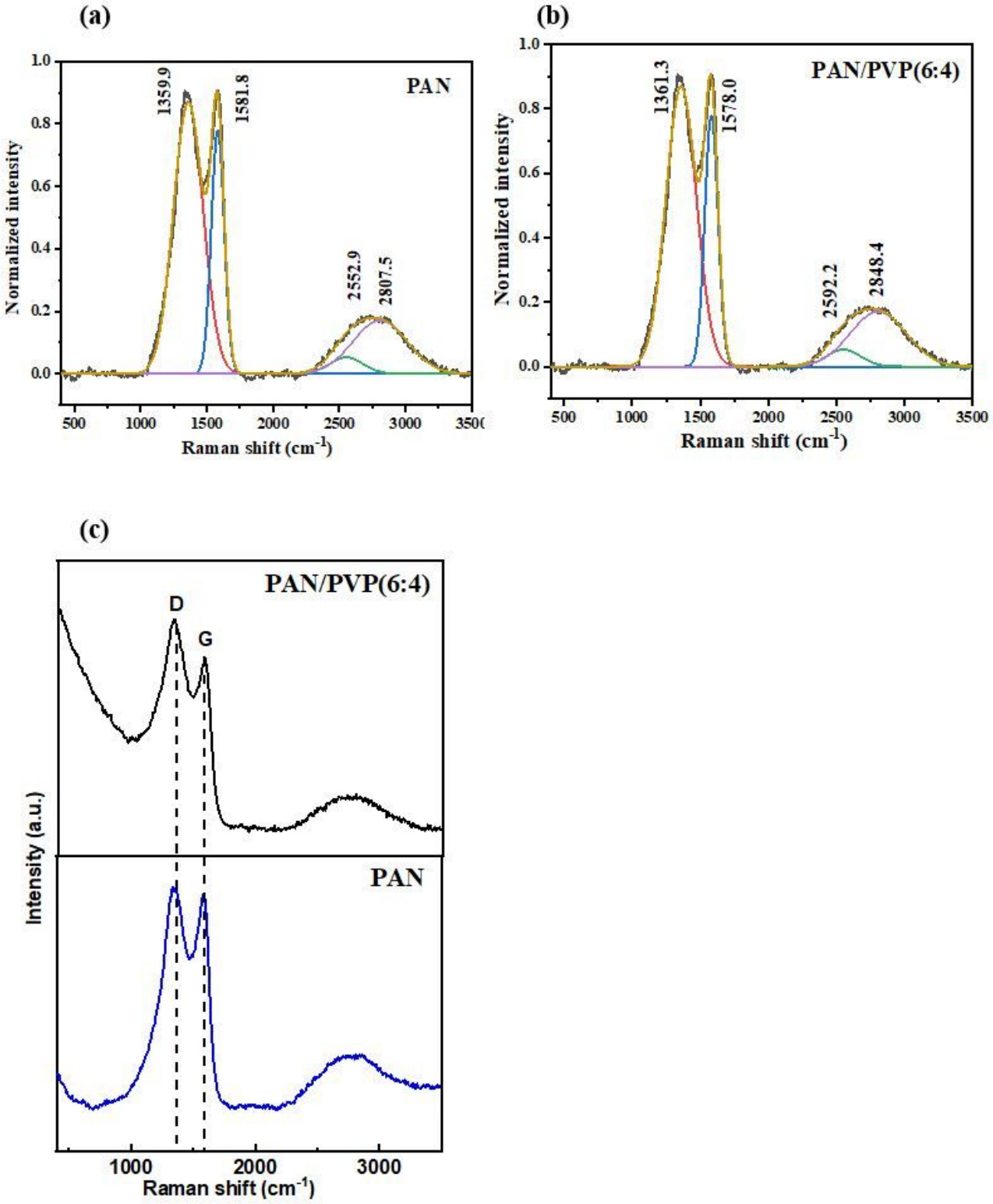

Figure 8

Raman Fitting curves of carbon nanofiber carbonized nanofibers at 800°C for 2 h. (a) PAN and (b) PAN/PVP (6:4). Raman spectra of (c) PAN and PAN/PVP (6:4).

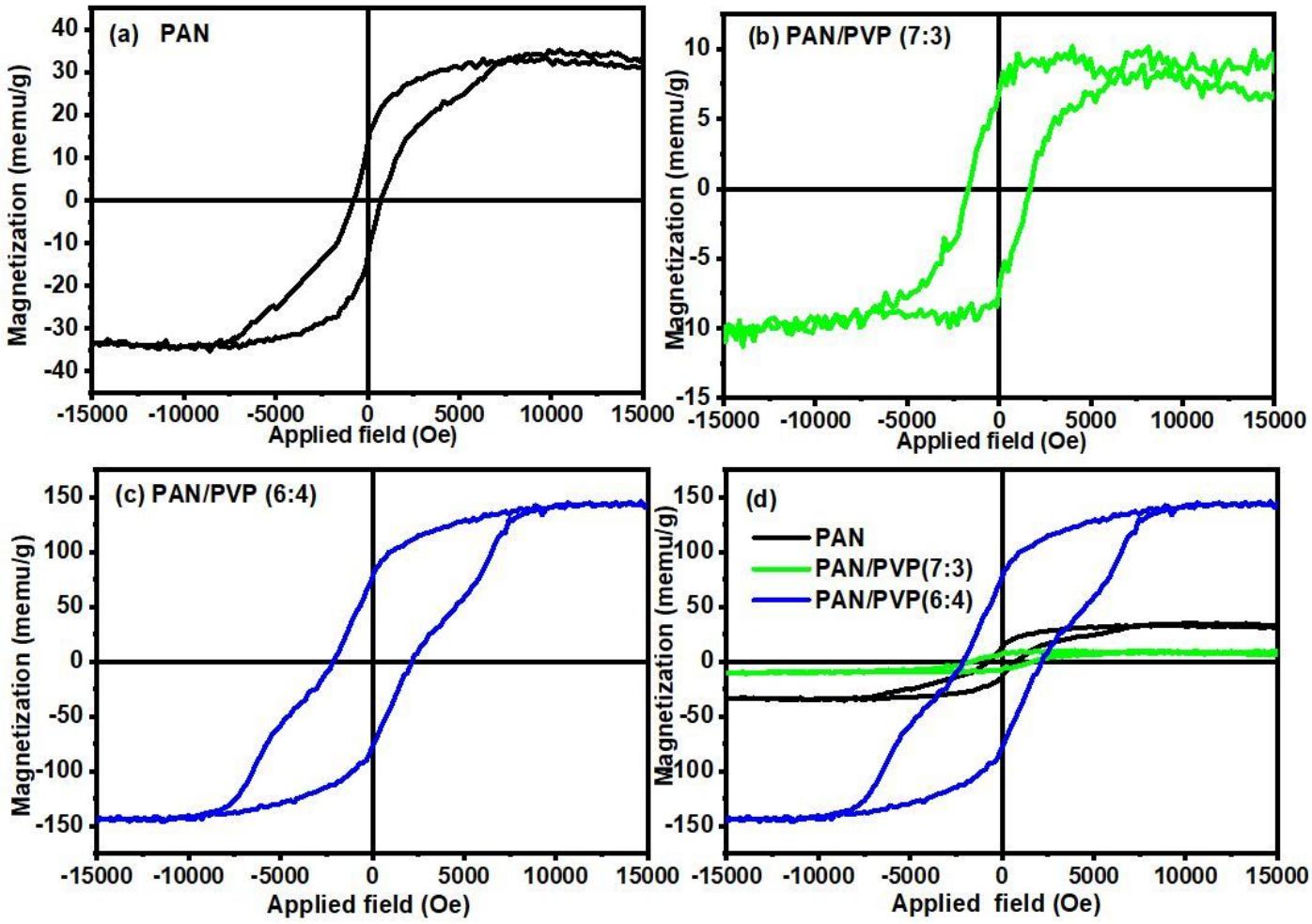

Figure 9

Magnetization of carbon nanofiber from PAN, PAN/PVP (7:3) and PAN/ PVP (6:4) in different ratio carbonized nanofibers at 800°C for 2 h. as a function of field at 300 K.